Polymerization effects and localized electronic states in condensed-phase eumelanin

L. Sangaletti,[1] P. Borghetti,[1] P. Ghosh,[2] S. Pagliara,[1] P. Vilmercati,[3] C. Castellarin-Cudia,[3] L. Floreano,[4] A. Cossaro,[4] A. Verdini,[4] R. Gebauer,[2,5] and A. Goldoni[3]

[1]*Dipartimento di Matematica e Fisica, Università Cattolica, via dei Musei 41, 25121 Brescia, Italy*

[2]*The Abdus Salam International Centre for Theoretical Physics (ICTP), Trieste, Italy*

[3]*Sincrotrone Trieste ScPA, Basovizza, Trieste, Italy*

[4]*CNR–TASC, Basovizza, Trieste, Italy*

[5]*INFM–DEMOCRITOS National Simulation Center, Trieste, Italy*

(Received 26 July 2009; published 17 November 2009)

The electronic structure of eumelanin thin films has been investigated by means of x-ray absorption and photoemission spectroscopies. The main features of the experimental data are interpreted on the basis of density-functional calculations for the isolated monomers participating to the eumelanin macromolecule. In order to single out the polymerization effects, we followed a bottom-up scaling approach to establish the minimum supramolecular level of organization that can provide a consistent spectroscopical picture of an altogether complex and highly disordered system. A tetramer macrocycle, made by three hydroquinones and one indolequinone, is found to reproduce the observed polymerization effects at the N *K* edge, while preserving the experimental spectral weight among the different monomers. This tetramer is different from that predicted for the synthesis from isolated monomers, providing an experimental evidence of the role of the reaction path on the stabilization of macrocycles in condensed-phase eumelanin.

DOI: 10.1103/PhysRevB.80.174203 PACS number(s): 71.20.Rv, 61.43.−j, 68.55.am, 71.15.Mb

I. INTRODUCTION

In spite of the importance of eumelanin from a biological and medical perspective, that has motivated many decades of research from biochemists and the biology community,[1–3] the structure, composition, and aggregation behavior of this class of pigments in the condensed phase is far from being thoroughly elucidated. In the condensed phase, eumelanin is usually described as an intrinsically disordered system, with a partial interlayer structural ordering, due to the stacking of oligomeric units (hereafter denoted as protomolecules) in a direction perpendicular to the monomer molecular plane.[4] At the primary level, it is fairly accepted that eumelanins are macromolecules of 5,6-dihydroxyindole (DHI, also known as HQ) and 5,6-dihydroxyindole-2-carboxylic acid and their various oxidized forms (semiquinone, QI, and indolequinone, IQ).[5] However, the way the single monomers are brought together to form the protomolecules has not yet been univocally identified. This is a fundamental issue to clarify, being the starting point for the construction of consistent structure-property-function relationships. The chemical structure of protomolecules, then, has important consequences on the electronic properties. In fact, the intrinsic chemical disorder (i.e., the superposition of different building blocks) and polymerization effects between different or like monomers may result in a rather broad spectral weight, without the sharp features characteristic of molecular levels of isolated molecules. Actually, polymerization is recognized as a central issue in the study of the electronic structure of melanins to such an extent that recent experimental studies have been carried out with the aim to grow single crystals containing eumelanin monomers by inhibiting the polymerization through the addition of suitable side groups.[6]

First-principles density-functional theory (DFT) calculations of the electronic structure of the melanin monomers[7,8] and model oligomers[9] have been published lately. Even if synthetic methods of preparing isolated monomers of DHI are available, it is not simple to test these calculations because these molecules are highly unstable and spontaneously polymerize in an oxidizing environment. Moreover, the feasibility of soft x-ray spectroscopy measurements of electronic properties of eumelanin in condensed phase has been tested only recently by studying eumelanin aggregates obtained by dispersion of powders in water droplets deposited onto copper substrates.[10]

Aim of the present study is the experimental and theoretical investigation of polymerization effects on the electronic properties of high-quality eumelanin thin films. The films have been prepared by drop casting from a solution of melanin powder aggregates in dimethyl sulfoxide (DMSO) and can be regarded as reference samples for the study of eumelanin in condensed phase. Indeed, they resulted to be homogeneous, flat on a nanometric scale, and virtually free from contamination arising from the solvent (mainly sulfur from DMSO). The experimental photoemission and absorption spectra have been compared to density-functional calculations of the occupied and unoccupied electronic states of single monomers and protomolecules. This evaluation is rather important because, owing to the inherent heterogeneity in the natural material and the difficulties associated with chemical analysis of the full macromolecular system, a *bottom-up* molecular approach may be the way to reach a final assessment of the melanin electronic properties.

II. EXPERIMENTAL AND COMPUTATIONAL DETAILS

Commercially available melanin powders (Sigma-Aldrich, cat. no. M8631), prepared by oxidation of tyrosine with hydrogen peroxide, have been used for the experiment. Atomic force microscopy imaging showed that eumelanin dissolved in DMSO and deposited by drop casting on indium tin oxide (ITO) covered glass substrates provided quite homogeneous films that did not display charging effects upon

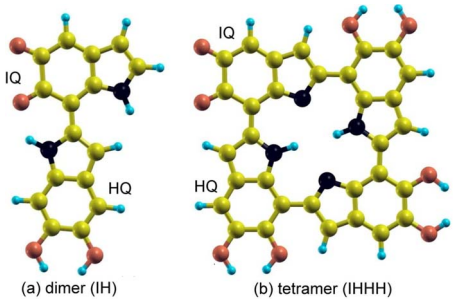

FIG. 1. (Color online) Model protomolecules for eumelanin: (a) a dimer composed of IH) and (b) IHHH tetramer (gold=C, red =O, black=N, and light blue=H).

photoionization, with a thickness of about 80–100 nm, and a reduced roughness (about 0.67 nm rms). These films have therefore been selected for the spectroscopy experiments. Raman spectroscopy was also used to estimate the relative content of basic monomers in our films, as was done for aggregates deposited onto Cu substrates.[10] The x-ray absorption spectroscopy (XAS) and soft x-ray photoemission spectroscopy spectra have been measured at the ALOISA beamline of the ELETTRA synchrotron light source in Trieste (Italy), whereas sample preparation and characterization was carried out at the Surface Science and Spectroscopy Laboratory of the Catholic University (Brescia, Italy).

The geometry and electronic properties of the monomers and the oligomers in the gas phase have been studied using the pseudopotential DFT-based QUANTUM-ESPRESSO package.[11] The monomers (cubic box of side 13.75 Å), the IQ-HQ (IH) dimer (box dimensions $13.75 \times 19.26 \times 13.75$ Å^3) and the IQ-HQ-HQ-HQ (IHHH) and QI-IQ-QI-IQ (QIQI) tetramers (box dimensions $19.26 \times 19.26 \times 13.75$ Å^3) were placed in large boxes to ensure negligible interactions between the periodic images. For all the cases the molecules lie in the *xy* plane (Fig. 1). Brillouin-zone integrations have been performed using Γ point only. We have used the Perdew-Burke-Ernzerhof[12] form of generalized gradient approximation for the exchange-correlation energies. Ground-state geometries and electronic structure of the monomers and oligomers have been calculated using ultrasoft pseudopotentials (UPP) (Ref. 13) and cutoffs of 25 and 300 Ry for the plane-wave basis set and the augmentation charge introduced by UPP, respectively.

Within the dipole approximation, the spectral intensity $[I(\epsilon)]$ of the x-ray absorption spectra is given by

$$I(\epsilon) \propto \sum_f |\langle \psi_{1s}|\mathbf{r}|\psi_f\rangle|^2 \delta(\epsilon_f - \epsilon_{1s} - \epsilon), \quad (1)$$

where $\mathbf{r}$ is the position operator, ϵ is the energy of the incident x ray, ϵ_f and ψ_f are the Kohn-Sham eigenvalue and eigenfunction, respectively, of the fth conduction band of the excited molecule, respectively, ϵ_{1s} and ψ_{1s} are the energy eigenvalue and the energy eigenfunction of the 1*s* level of the element whose core-level spectra is to be calculated. The summation f extends to all the energy levels above the highest-occupied molecular orbital of the molecule. The delta function has been replaced by a Gaussian of width 0.24 eV.

Since we are using pseudopotential-based DFT, in which the core electrons and the strong nuclear potential have been replaced with a pseudopotential, we do not have information regarding the ψ_{1s} orbital of the atom whose spectra we are interested in calculating, when it forms a molecule through interaction with other atoms. However, based on the assumption that the core orbitals are relatively unaffected by differences in the chemical surroundings of the atoms, the ψ_{1s} orbital can be obtained from an all electron calculation of the atom and can be used in evaluating the transition matrix elements. While there are more sophisticated approaches for obtaining the ψ_{1s} orbital,[14,15] this approach yields results which are in reasonably good agreement with the experiments.

The electron excitation can be modeled by the Slater's transition state theory,[16,17] where half an electron can be promoted from a core state to the excited state. The difference between the final and initial values correspond to the excitation energies.[18] The excitation energies can also be evaluated by calculating the differences in total energy in which a *whole* electron is promoted from a core state to an excited state. This is also called the ΔSCF approach. However, for both the above mentioned approaches, it is necessary to do a DFT calculation for each individual excited state, thus making the procedures computationally demanding. A less expensive alternative is to calculate the virtual orbitals of the system in the presence of a half core hole (HCH) or a full core hole (FCH) on the absorbing nucleus. The excited electron is usually removed from the system.[19–21] Since previous calculations suggests that for molecules and clusters the HCH technique provides a better agreement with experiment, while for condensed phase the FCH is a better approximation,[19–26] we use the HCH technique in order to calculate the x-ray absorption spectra. It should be noted that due to the presence of the core hole in the pseudopotential of the excited atom, such calculations model the relaxation of the valence electrons following the excitation.

We have performed spectral calculations for C and N. For the excited atoms, we have used Troullier-Martin-type norm-conserving pseudopotential with a wave function cut off of 70 Ry. The pseudopotentials have been generated using the atomic code which is also a part of the QUANTUM-ESPRESSO package. We have used electronic configurations of $1s^{1.5}2s^22p^2$ and $1s^{1.5}2s^22p^3$, and cut off radius of 1.20 and 1.23 a.u. (for $l=0$ and $l=1$, where the later channel is local) for C and N, respectively. In such pseudopotential-based calculations the energy of the core states is not directly available. Therefore absolute excitation energies are not computed. Our calculations provide relative excitation energies, and throughout the paper we shift the excitation energies by an arbitrary constant for better visual comparison with experiment. The computed spectra of different molecules are aligned with respect to each other using the vacuum level as a reference.

III. RESULTS AND DISCUSSION

A. Raman and optical spectroscopies

In agreement with previous results,[10] Raman measurements (Fig. 2) indicate that the eumelanin spectrum does not

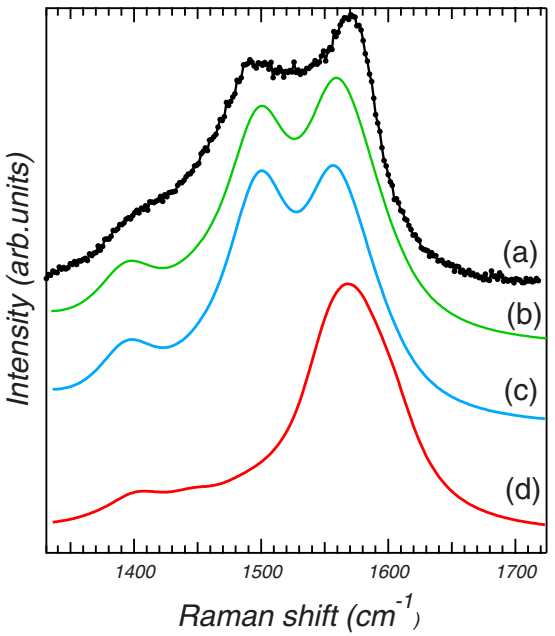

FIG. 2. (Color online) Measured Raman spectrum of the melanin thin films on (a) ITO compared with the best fit based on a linear combination of (b) monomers and with the calculated spectra of (c) IHHH and (d) QIQI.

depend on the sample preparation, but can be superposed to that of precursor powders. Furthermore, the Raman spectrum does not change with time over at least one year after the first measurements, and virtually identical spectra have been collected from different batches purchased over the years. This is assumed as a proof of the sample stability and therefore of the reproducibility of the experimental conditions. The best fit in Fig. 2 is obtained through a linear combination of the HQ monomer (about 70%) and of the IQ monomer (about 30%) while QI is virtually absent.

The wavelength-dependent optical-density (OD) spectrum in the UV-visible range data is shown in Fig. 3, while in the inset the square root of the OD has been fit with a straight

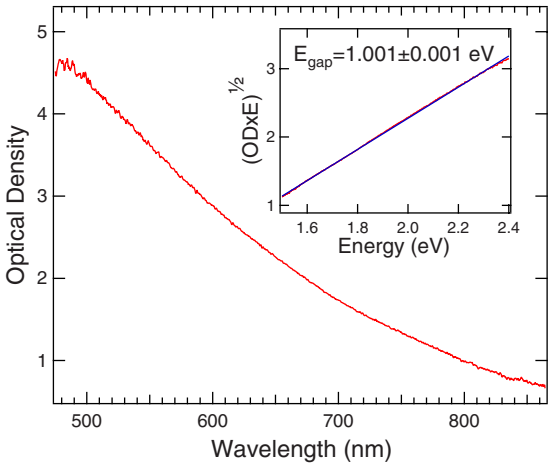

FIG. 3. (Color online) Absorption spectrum of eumelanin deposited on a ITO in the visible range. In order to estimate the band gap, the $OD^{1/2}$ has been fit with a straight line.

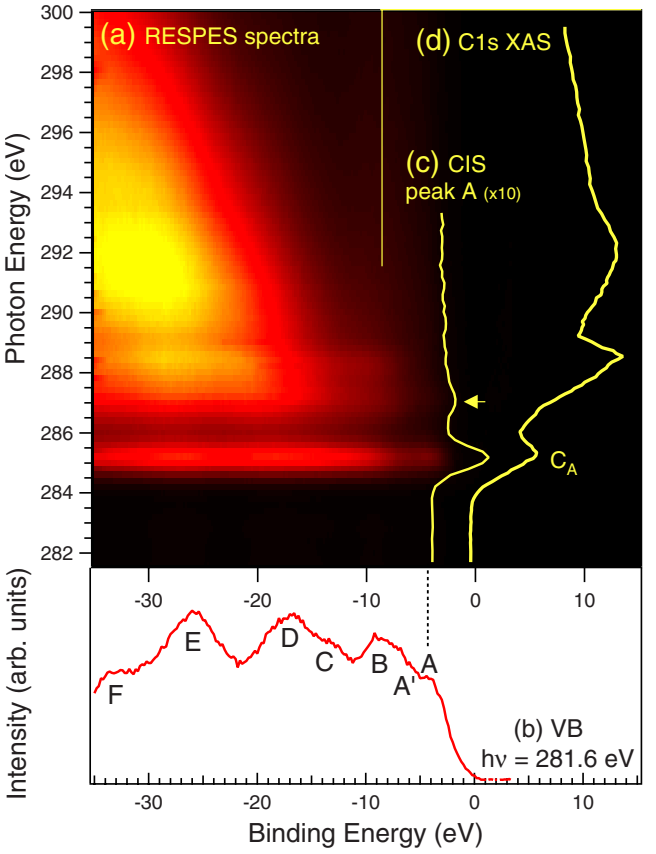

FIG. 4. (Color online) (a) RESPES data of melanin films deposited on ITO collected across the C 1*s* absorption threshold. Labels A–F denote the binding energies of the spectral features identified in spectrum (b), which shows the valence band collected with $h\nu = 281.6$ eV photon energy. (c) Intensity profile, also known as CIS (i.e., constant ionization state), of peak A in the valence band when the photon energy is scanned through the C 1*s* absorption threshold. (d) C 1*s* XAS spectrum.

line in order to estimate the band gap, as is usually done in amorphous semiconductors.[27] From the fit, an energy gap of about 1 eV has been evaluated for the present samples.

B. Photoemission spectroscopies and density of states

Figure 4(a) shows the valence-band resonant photoemission spectroscopy (RESPES) obtained by scanning the photon energy across the C 1*s* absorption threshold, from 281.6 to 302 eV. The C 1*s* XAS spectrum measured during the RESPES scan is also shown in Fig. 4(d) while, as an example, the valence-band spectrum collected with $h\nu = 281.6$ eV photon energy is displayed in Fig. 4(b). From RESPES data, the constant initial state (CIS) profiles of several peaks can be extracted, as we did for peak A in the valence band [Fig. 4(c)]. The first resonance in RESPES spectra is detected at about $h\nu = 285.2$ eV [peak C_A in Fig. 4(d)], for which all valence-band features, labeled from A to F in Fig. 4(b), show an intensity enhancement. In the XAS spectrum, the lowest-lying peak C_A can be ascribed to excitation into π^* empty orbitals, as is usually found in hydrocarbon rings,[28] while in the region at higher photon energies

a significant contribution from σ^* states is predicted. Beyond this enhancement an Auger emission with a clear dispersive behavior on the binding energy (BE) scale (i.e., a normal Auger emission) appears. The analysis of the CIS spectrum reveals that the pure resonant behavior observed for feature A involves photon energies exciting the first π^* transition and, to a minor extent, the transition at 287.2 eV [indicated by an arrow in Fig. 4(c)]. This suggests that when an electron is excited from the C 1*s* core level to these states, it remains localized for a time long enough to allow interference between the autoionization decay channel and the direct photoemission channel. This effect was also observed in RESPES data from benzoic acid thin films on $TiO_2(110)$.[29] In turn, when the electron is excited into higher empty states (overlapping with σ bands) no resonance is detected, suggesting a prompt delocalization of the excited electron compared to the core-hole lifetime. Furthermore, the resonant behavior of peak A in the valence band indicates that its origin has to be related to occupied π-type orbitals.

Figure 5 shows the valence-band photoemission spectrum obtained with (a) $h\nu$=281.6 eV photons from the synchrotron, as well as with (b) an Al $K\alpha$ x-ray source, i.e., $h\nu$ =1486.6 eV. Unlike the featureless UV-VIS optical spectrum (Fig. 3) typical of melanin samples,[30] the features observed in the valence-band photoemission spectrum are still well separated from one another, enabling an effective comparison with theoretical calculations. In Figs. 5(a) and 5(b) several spectral features, labeled as A to F, can be singled out, indicating that the molecular character of the electronic states is preserved in the solid state. First of all, it should be observed that the linewidth of all experimental bands does not change with the experimental resolution, which is about 150 meV for synchrotron radiation and about 1 eV for the Al $K\alpha$ source. This suggests that the bandwidth is an intrinsic effect of the thin films, very likely due to polymerization effects. On the basis of a previous comparison with the calculated density of states (DOS) of HQ (the prevalent monomer) through a projection on several orbitals,[10] the overall energy range can be divided into three regions, separated by vertical dashed lines in Fig. 5. The first ranges from BE=0 to BE=10 eV and is characterized by a relevant contribution from carbon π orbitals, that is, not found elsewhere in the calculated spectrum. The second region ranges from 10 to 20 eV, with a relevant contribution from carbon σ orbitals. Finally, the third region ranges from 20 to 30 eV, with a prevalent contribution from carbon, nitrogen, and oxygen shallow core levels. The calculated HQ DOS itself [Fig. 5(f)] catches the main experimental features in the valence-band region. The IQ DOS [Fig. 5(g)] also seems to agree with the experimental data with a worse accordance with respect to HQ in the shallow core-level region (i.e., below experimental peak E).

As a first exploration of the polymerization effects, we have considered the tetramers IHHH [Fig. 1(b)] and QIQI, both of which have an inner porphyrinlike ring according to the model proposed by Kaxiras *et al.*[9] It is important to observe that in IHHH the IQ:HQ ratio (25:75) is quite close to that estimated from Raman data (30:70), indicating that IHHH tetramer could be regarded as the most abundant and stable aggregation form of eumelanin in the present samples,

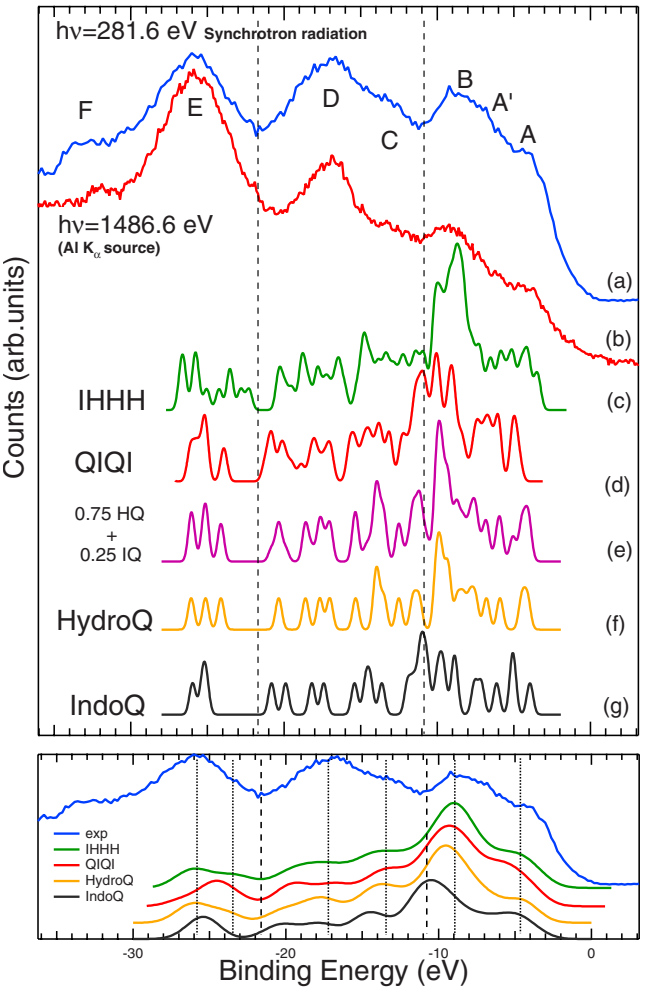

FIG. 5. (Color online) Top panel: photoemission spectra of synthetic eumelanin collected by exciting the sample with (a) $h\nu$ =281.6 eV and (b) $h\nu$=1486.6 eV photon energies. The main bands are labeled from A to F. Calculated density of states of the tetramers (c) IHHH and (d) QIQI, of a weighted mix of (e) IQ and HQ, and of the monomers (f) HQ and (g) IQ. Bottom panel: calculated spectra convoluted with a Gaussian function (FWHM =1.0 eV).

prepared by oxidation of tyrosine with hydrogen peroxide. Actually the calculated Raman spectrum for IHHH [Fig. 2(c)] is quite similar to that obtained from the best fit [Fig. 2(b)]. On the other side, the Raman spectrum calculated on the basis of the relative weight of monomers in QIQI [Fig. 2(d)] is quite far from the experimental data, and therefore exclude significant contributions from QIQI macrocycles in the present samples. However, according to Kaxiras *et al.*, IHHH has the largest negative formation energy while QIQI has the largest positive formation energy. Their results suggests that, at least in gas phase, formation of QIQI is more probable than IHHH. Our calculations of the formation energy of IHHH and QIQI yield values of −3.44 and 0.81 eV, respectively. Although the results agree qualitatively with those of Ref. 9, the differences in the absolute values of formation energies may be due to the use of different types of exchange-correlation functionals and pseudopotentials. Since the composition of the films obtained from Raman

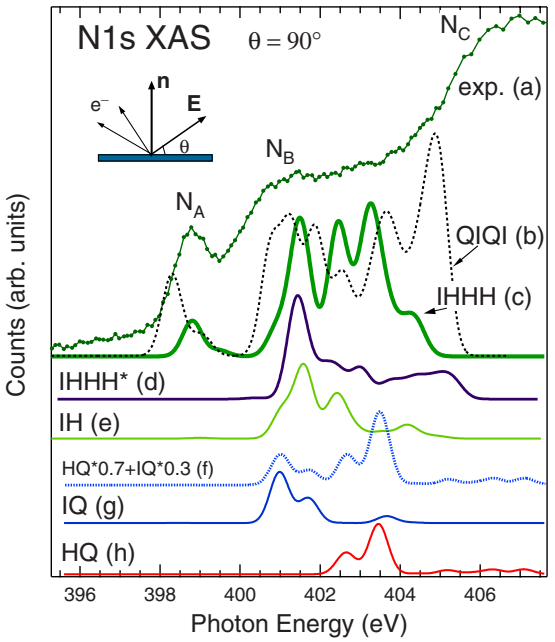

FIG. 6. (Color online) (a) Experimental N 1*s* XAS spectrum; calculated XAS spectra of the (b) QIQI, and (c) IHHH tetramers, the IHHH tetramer with four hydrogens in the ring [(d) IHHH*], the dimer (e) IH, the spectrum resulting from the linear combination (f) HQ*0.7+IQ*0.3, the monomer (g) IQ, and the monomer (h) HQ. The experimental spectrum has been collected across the N 1*s* *K* edge at nearly grazing photon incidence with linear polarization of light perpendicular to the thin-film surface.

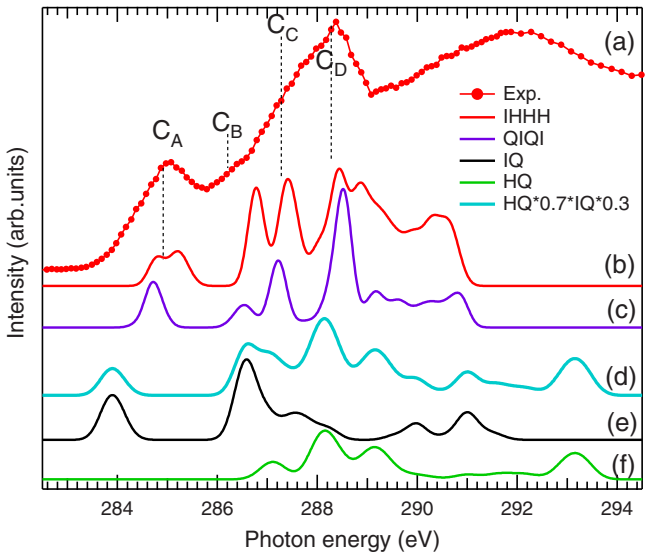

FIG. 7. (Color online) (a) C 1*s* XAS spectrum compared with the calculated XAS spectra of the (b) IHHH, and (c) QIQI tetramers, the spectrum resulting from the linear combination (d) HQ*0.7+IQ*0.3, the monomer (e) IQ and the monomer (f) HQ. The experimental conditions are those specified for Fig. 6.

measurements indicate the presence of IHHH, while a comparison of the relative energies of IHHH and QIQI (calculations for which have been done neglecting the effect of the chemical environment during the formation process) favors the presence of the latter, it seems that during the synthesis in the condensed phase of the present melanin samples, the reaction path stabilizes the IHHH tetramer. To test this we have done calculations for the occupied DOS and the C 1*s* and N 1*s* XAS, the results of which are presented in the following, for both IHHH and QIQI. Another important issue regarding the geometry of tetramers is the H termination of the N atoms inside the ring. For IHHH we considered two cases: (a) in which the all the N atoms are terminated with H (IHHH*) and (b) in which only two of the N atoms are H terminated (IHHH). In agreement with Ref. 9, we find that (b) is energetically more favorable than (a) which has a formation energy of −4.88 eV.

When examining the DOS of the IHHH and QIQI tetramers [Figs. 5(c) and 5(d)], the agreement with experimental data is better than the case of isolated monomers. In particular, in the region below peak A a broad band is found for IHHH DOS and likewise, also the contribution in the shallow core-level region is now spread in a larger BE range. In order to show the extent of polymerization effects in the IHHH tetramer, the IHHH DOS is compared to that of a linear combination of HQ and IQ [Fig. 5(e)], accounting the same ratio as in the IHHH tetramer. It is clear that a linear combination still retains a monomerlike structure and the electronic states in the different specific regions are not such spread as in the case of tetramer. Moreover among the two tetramers, the DOS of IHHH is in better agreement with the experimental one, suggesting the presence of IHHH than QIQI in the sample. This is also clear when the calculated spectra are convoluted with a Gaussian function (FWHM = 1.0 eV), as shown in the bottom panel of Fig. 5. Although the calculated spectra show a similar sequence of main features, the fitting to the experimental data evidences differences on the intensity and energy of the main spectral features, which make the theoretical spectrum of the IHHH tetramer the closer to the experimental data, while the worse agreement is given by the isolated IQ monomer.

C. X-ray absorption spectroscopy

A distinct evidence of polymerization effects is obtained by analyzing the N 1*s* XAS spectrum. Incidentally, we observe that this analysis does not require a deconvolution of the spectral weight on different atoms as in the case of C, as each monomer contains one single N atom. The experimental data are dominated by the two features N_A and N_B, respectively, at 398.7 and 400.7 eV [Fig. 6(a)], which have a clear counterpart in the calculated XAS spectrum of QIQI and IHHH [Figs. 6(b) and 6(c), respectively]. While the first feature results from transitions to the lowest unoccupied molecular orbital (LUMO) of the tetramers, the second feature is due to several transitions to other unoccupied states higher in energy.

It is quite interesting to observe that the peak at 398 eV does not appear in the calculated XAS of the monomers [Figs. 6(g) and 6(h)], the linear combination HQ*0.7 +IQ*0.3 of the two monomers [Fig. 6(f)], the dimer [Fig. 6(e)] and in IHHH* [Fig. 6(d)]. This indicates that: (i) presence of the N_A peak can be reproduced in the calculated XAS spectrum provided that polymerization has occurred in eu-

melanin and (ii) presence of more H atoms in the ring makes the tetramer unstable due to steric repulsions.

Finally we consider the C 1*s* spectrum (Fig. 7). As already observed, the experimental C 1*s* XAS spectrum has a sharp peak C_A at 285.2 eV followed by three features C_B, C_C, and C_D detected at higher photon energies. This spectrum has been compared with the ones computed for the monomers, the linear combination of the two monomers and the tetramers [Figs. 7(b)–7(f)]. The calculated spectra of HQ [Fig. 7(f)] is in worse agreement with the experimental one with the first peak missing. Though the spectra for IQ [Fig. 7(e)] has features similar to the experimental one, the relative positions of the peaks are quite different from the measured spectra. A similar behavior is observed also for the linear combination $HQ^*0.7+IQ^*0.3$ of the two monomers [Fig. 7(d)]. For both the tetramers [Figs. 7(b) and 7(c)], the calculated spectra are in good agreement with the experimental data. C_A results due to transitions to the π^*-like LUMO and LUMO+1 as is usually found in hydrocarbon rings,[28] while in the region at higher photon energies there is significant contribution from σ^* states.

IV. CONCLUSIONS

In conclusion, by using soft x-ray spectroscopies, we have been able to probe the density of states of both occupied and unoccupied electronic levels of eumelanin in the condensed phase. A good agreement with the experimental data is found with the calculated DOS of the HQ monomer but a better agreement is found when the IHHH tetramer with two N atoms terminated with H atoms is considered. This shows to which extent the calculated electronic structure of single monomers catches the main features of solid-state aggregates. Due to polymerization, the local environment of the N atoms differs completely from that of the individual monomers (suggested by absence of the first feature in the N 1*s* XAS of the monomers). Moreover the Raman spectroscopy measurements and a comparison between the experimental and the calculated XAS spectra suggest that during the synthesis of condensed phase eumelanin from the oxidation of tyrosine, the IHHH tetramer is stabilized, unlike the calculations on synthesis from gas phase where the QIQI tetramer resulted to be the more stable,[9] indicating that the exploration of the more stable forms of eumelanin protomolecules cannot be carried out without considering the environmental conditions of the melanin synthesis processes.

ACKNOWLEDGMENTS

L.S. wishes to acknowledge Marco Bettinelli for helpful discussions and suggestions.

[1] H. Z. Hill and G. J. Hill, Pigment Cell Res. **1**, 163 (1987).
[2] C. G. Burkhart and C. N. Burkhart, Int. J. Dermatol. **44**, 340 (2005).
[3] F. A. Zucca, G. Giavieri, M. Gallorini, A. Albertini, M. Toscani, G. Pezzoli, R. Lucius, H. Wilms, D. Sulzer, S. Ito, K. Wakamatsu, and L. Zecca, Pigment Cell Res. **17**, 610 (2004).
[4] C. M. R. Clancy and J. D. Simon, Biochemistry **40**, 13353 (2001).
[5] S. Ito, Biochim. Biophys. Acta **883**, 155 (1986).
[6] S. P. Nighswander-Rempel, I. B. Mahadevan, P. V. Bernhardt, J. Butcher, and P. Meredith, Photochem. Photobiol. **84**, 620 (2008).
[7] B. J. Powell, T. Baruah, N. Bernstein, K. Brake, R. H. Mckenzie, P. Meredith, and M. R. Pederson, J. Chem. Phys. **120**, 8608 (2004).
[8] B. J. Powell, Chem. Phys. Lett. **402**, 111 (2005).
[9] E. Kaxiras, A. Tsolakidis, G. Zonios, and S. Meng, Phys. Rev. Lett. **97**, 218102 (2006).
[10] L. Sangaletti, S. Pagliara, P. Vilmercati, C. Castellarin-Cudia, P. Borghetti, P. Galinetto, R. Gebauer, and A. Goldoni, J. Phys. Chem. B **111**, 5372 (2007).
[11] Paolo Giannozzi *et al.*, J. Phys.: Condens. Matter **21**, 395502 (2009); URL: http://www.quantum-espresso.org
[12] J. P. Perdew, K. Burke, and M. Ernzerhof, Phys. Rev. Lett. **77**, 3865 (1996).
[13] D. Vanderbilt, Phys. Rev. B **41**, 7892 (1990).
[14] P. E. Blöchl, Phys. Rev. B **50**, 17953 (1994).
[15] B. Hetényi, F. De Angelis, P. Giannozzi, and R. Car, J. Chem. Phys. **115**, 5791 (2001).
[16] J. C. Slater, Adv. Quantum Chem. **6**, 1 (1972).
[17] J. C. Slater and K. H. Johnsson, Phys. Rev. B **5**, 844 (1972).
[18] J. F. Janak, Phys. Rev. B **18**, 7165 (1978).
[19] P. Rez, J. R. Alvarez, and C. Pickard, Ultramicroscopy **78**, 175 (1999).
[20] L. Triguero, L. G. M. Pettersson, and H. Ågren, Phys. Rev. B **58**, 8097 (1998).
[21] R. Buczko, G. Duscher, S. J. Pennycook, and S. T. Pantelides, Phys. Rev. Lett. **85**, 2168 (2000).
[22] B. Hetényi, F. De Angelis, P. Giannozzi, and R. Car, J. Chem. Phys. **120**, 8632 (2004).
[23] I. Tanaka, H. Araki, M. Yoshiya, T. Mizoguchi, K. Ogasawara, and H. Adachi, Phys. Rev. B **60**, 4944 (1999).
[24] K. Lie, R. Hoier, and R. Brydson, Phys. Rev. B **61**, 1786 (2000).
[25] C. Elsasser and S. Kostlmeier, Ultramicroscopy **86**, 325 (2001).
[26] M. Cavalleri, M. Odelius, A. Nilsson, and L. G. M. Pettersson, J. Chem. Phys. **121**, 10065 (2004).
[27] N. F. Mott and E. A. Davies, *Electronic Process in Non-Crystalline Materials* (Clarendon, Oxford, 1979).
[28] J. Stöhr, *NEXAFS Spectroscopy* (Springer-Verlag, Berlin, 1996).
[29] J. Schnadt, J. N. O'Shea, L. Patthey, J. Krempasky, N. Mårtensson, and P. A. Brühwiler, Phys. Rev. B **67**, 235420 (2003).
[30] See, e.g., Paul Meredith, Ben J. Powell, Jennifer Riesz, Stephen P. Nighswander-Rempel, Mark R. Pederson, and Evan G. Moore, Soft Matter **2**, 37 (2006), and references therein.